Tumour acidosis evaluated in vivo by MRI-CEST pH imaging reveals breast cancer metastatic potential

Title page

Title

MRI-CEST pH imaging: a new tool for assessing *in vivo* the early metabolic response and onset of resistance to dichloroacetate in a murine breast cancer model

Running title

CEST-pH imaging of glycolysis inhibition by DCA

Authors:

Annasofia Anemone[1,2], Lorena Consolino[1,2], Laura Conti[1], Francesca Reineri[1,2], Federica Cavallo[1], Silvio Aime[1,2] and Dario Livio Longo[2,3]

[1]Dipartimento di Biotecnologie Molecolari e Scienze per la Salute, Università degli Studi di Torino, 10126, Torino, Italy

[2]Molecular Imaging Center, Università degli Studi di Torino, 10126, Torino, Italy

[3]Istituto di Biostrutture e Bioimmagini (CNR), Centro di Biotecnologie Molecolari, 10126, Torino, Italy

Corresponding author:

Dario Livio Longo, Istituto di Biostrutture e Bioimmagini, (CNR) c/o Centro di Biotecnologie Molecolari, Via Nizza 52, 10126, Torino, Italy

Phone: +39-011-6706473, Fax: +39-011-6706487, email: dario.longo@unito.it.

Abstract

Background

Dichloroacetate (DCA) can reverse the glycolytic phenotype in cancer cells that is responsible of increased lactate production and extracellular pH acidification. We examined whether MRI-CEST pH mapping can monitor *in vivo* tumour acidosis to assess treatment response to DCA.

Methods

Cell viability and extracellular pH were assessed in TS/A breast cancer cells treated with 1-10 mM DCA for 24 h in normoxia or hypoxia (1% O_2) conditions. Extracellular tumour pH values were measured *in vivo* by MRI-CEST pH mapping of TS/A tumour bearing mice before, three days and fifteen days after DCA or saline treatment.

Results

Reduced extracellular acidification and viability was observed in DCA-treated TS/A cells. Tumour bearing mice showed a marked and significant increase of tumour extracellular pH at 3 days post DCA treatment, reflecting DCA-induced glycolysis inhibition, as confirmed by reduced lactate production. After 15 days of DCA treatment, the onset of resistance to DCA was observed, with recover of tumour extracellular acidification and lactate levels that returned to control values. A significant correlation was observed between the tumour extracellular pH and lactate levels ($r=-0.97$, $P<0.05$).

Conclusions

MRI-CEST pH imaging appears a promising tool to monitor the early response and efficacy of cancer metabolic targeting drugs.

Keywords

Glycolysis, metabolic inhibitor, dichloroacetate, MRI CEST-pH, breast cancer, extracellular pH, iopamidol, tumour, acidosis, lactate, imaging, chemical exchange saturation transfer.

Introduction

It is well known that the extracellular pH (pHe) within the microenvironment of tumours is significantly lower (more acidic) compared with that of normal tissues (Gerweck & Seetharaman, 1996). Although several factors play a role in this acidification, it is well accepted that the major contribution arises from a shift in the ATP generation from oxidative phosphorylation to aerobic glycolysis, even under normal oxygen concentrations (Warburg *et al*, 1927). In this contest, poor vascularisation and increased activity of plasma membrane ion pumps and transporters (H^+-ATPases, the Na^+–H^+ exchanger NHE1 and the monocarboxylate–H^+ efflux co-transporters MCT1 and MCT4) (Webb *et al*, 2011) contribute to the extracellular acidification of most, but not all tumours. Many studies on solid tumours and in particular on breast tumours suggested that a glycolytic environment is associated with an antiapoptotic, pro-proliferative state and that lactic acidosis facilitates the breakdown of the extra-cellular matrix allowing expansion, increase of the metastatic potential and promotion of angiogenesis (Hashim *et al*, 2011). Therefore, novel drugs addressing specific aspects of the deregulated tumour metabolism have been proposed for inhibiting tumour growth and survival (Kinnaird & Michelakis, 2015).

Dichloroacetate (DCA), a mitochondria-targeting small molecule of 150 Da (Michelakis *et al*, 2008) used to treat patients with lactic acidosis, can reverse this cancer-specific metabolic remodelling. DCA inhibits pyruvate dehydrogenase kinase (PDK) whose expression is high in many cancers (McFate *et al*, 2008). PDK is a negative regulator of the pyruvate dehydrogenase complex (PDH) that catalyses oxidative decarboxylation of pyruvate to acetyl-CoA, which allows the entry of pyruvate into the tricarboxylic acid cycle (TCA or Krebs cycle) and away from lactate production. Therefore, PDK leads to an increased lactate production. DCA-mediated inhibition of PDK leads to the activation of PDH, increased metabolism of pyruvate to acetyl-CoA and decreased lactate production. Thus, DCA increases glucose oxidation promoting apoptosis and blocking tumour proliferation (Bonnet *et al*, 2007). Several clinical studies tested the DCA anti-tumour efficacy and its safety in patients with advanced solid tumours (Chu *et al*, 2015; Dunbar *et al*, 2014; Garon *et al*, 2014). Overall these studies reported that oral DCA is well tolerated and safe, it reduces lactate levels and it can act as an apoptosis sensitizer in combination with cytotoxic treatments.

Despite the specific mechanism of action of DCA on tumour glycolysis, tumour response to DCA treatment has conventionally been assessed through simple measurements of changes in tumour size using

morphological imaging techniques such as Computed Tomography (CT) or Magnetic Resonance Imaging (MRI). However, the assessment of changes in tumour volume does not provide indications on variations in tumour acidosis induced by metabolism-targeting drugs. Several MRI methods have been proposed for non-invasive measurements of *in vivo* tumour pH (Zhang *et al*, 2010). In particular, ^{31}P-magnetic resonance spectroscopy (^{31}P-MRS) allows measuring intracellular pH (pHi) from the chemical shift of endogenous phosphate and pHe from the chemical shift of exogenous indicators, such as 3-aminopropyl phosphonate (3-APP), but with poor spatial resolution (Gillies *et al*, 1994). Gd-based contrast agents that exhibit a pH-dependent relaxivity have been exploited for measuring tumour pH in a rat glioma model, but a limitation of this approach is related to the need of injecting two Gd-based contrast agents for accurate pH measurements (Garcia-Martin *et al*, 2006). Hyperpolarized ^{13}C bicarbonate can provide pHe map with high sensitivity (Gallagher *et al*, 2008), while several hyperpolarised molecules can provide insight into metabolism in both cells and animals (Reineri *et al*, 2015; Reineri *et al*, 2016; Serrao & Brindle, 2016; Viale *et al*, 2012). However, this technique is expensive, limited by low spatial resolution and requires sophisticated instrumentations that are not easily available in clinical setting.

Recently, Chemical Exchange Saturation Transfer (CEST) imaging has been proposed as a novel MRI-based technique and several pH-responsive agents have been considered for assessing tumour pHe (Hingorani *et al*, 2015). Among them, clinical approved radiographic contrast agents have been exploited for measuring pH and pathological-induced pH changes (Chen *et al*, 2014; Chen *et al*, 2015; Jones *et al*, 2015; Longo *et al*, 2013; Longo *et al*, 2011; Moon *et al*, 2015). In addition, MRI-CEST pH mapping was demonstrated to be an excellent tool to investigate the relationship between glycolysis and acidosis at clinical magnetic field (Longo *et al*, 2016a).

In this study, we investigated MRI-CEST pH mapping as a potential non-invasive biomarker of response following DCA treatment, evaluating changes in tumour acidosis in a murine breast cancer model.

Materials and Methods

In Vitro experiments

Cell culture

TS/A cells, derived from a spontaneous BALB/c mammary tumour (Nanni et al, 1983), were grown in RPMI 1640 medium supplemented with 10% fetal bovine serum (FBS), 100U/mL Penicillin and 100 µg/mL Streptomycin (Pen/Strep) and 2 mM L-Glutamine. 4T1 cells were purchased from American Type Culture Collection, ATCC and cultured as TS/A cells. TUBO cells are derived from a lobular carcinoma arising spontaneously in a BALB-neuT mouse (Lanzardo *et al*, 2016) and were grown in DMEM medium supplemented with 20% FBS and Pen/Strep.

J774 non-tumour cell line (purchased from ATCC) was grown in DMEM medium supplemented with 10% FBS, Pen/Strep and L-Glutamine. All the cell lines were cultured at 37 °C in a humidified atmosphere with 5% CO_2 .

Cell viability test

The cytotoxic effect of DCA (Sigma Aldrich, MO, USA) on cells was analysed with the CellTiter-Blue Cell Viability Assay (Promega Corporation, USA). Briefly, TS/A (5×10^3) cells were plated in 96-well culture plates and after 24 hours of incubation were treated with DCA (1mM, 5mM and 10mM) for 24 hours. The non-tumour cell line J774 (30×10^3) was used as control and treated in the same way. Afterwards, cells were washed with PBS and then CellTiter-Blue reagent was added to each well. Fluorescence was measured at 560Ex/590Em using a 96-well plate reader. Each assay was repeated at least three times.

pH measurement in normoxia and hypoxia condition

TS/A cells were seeded in culture plates at a density of 4×10^5 cells. After 24 hours of incubator in 20% O_2 (normoxia) or 1% O_2 (hypoxia) (New Brunswick™ Galaxy® 48 R, Eppendorf S.r.l., Italy) cells were treated with a solution of DCA (1mM, 5mM and 10mM) and let in the culture medium for additional 24 hours. Then the culture medium was collected and immediately the pH was measured using a pH meter (Hamilton® Slim Trode, GR, Switzerland) previously calibrated. The non-tumour cell line J774 underwent the same procedure. Each experiment was performed in triplicate.

FACS analysis

The cell cycle perturbations were analysed by Propidium Iodide (PI) DNA staining. TS/A cells (5x 10^5) were treated with DCA (1mM, 5mM and 10mM) for 24 hours. At the end of each treatment, cells were collected after a centrifugation at 1100 rpm for 5 minutes and then fixed in 70% ethanol for 3 minutes at 4°C. Ethanol-suspended cells were diluted with phosphate buffered saline (PBS) and then centrifuged at 1500 rpm for 5 minutes to remove residual ethanol. For cell cycle analysis, the pellets were suspended in 0.1mL of PBS containing 50 µg/mL of PI, 100µg/mL of RNase A and 0.05% of Triton X-100 and incubated at 37°C for 40 minutes. Cell cycle profiles were studied using a CyanADP flow cytometer and analysed with Summit 3.4 software (Beckman Coulter). Each assay was repeated a minimum of three times.

In Vivo **experiments**

Animal experiments

BALB/c female mice (Charles River Laboratories Italia S.r.l., Calco Italia) were maintained under specific pathogen free conditions in the animal facility of the Molecular Biotechnology Center, University of Turin, and treated in accordance with the University Ethical Committee and European guidelines under directive 2010/63.

Mice were inoculated subcutaneously with 2.5×10^5 TS/A mammary adenocarcinoma cells on both flanks. When the tumours were approximately $60mm^3$, TS/A tumour bearing mice were randomly divided in two groups: untreated group that received drinking water and intraperitoneal injections of PBS, and DCA-treated group that received DCA by oral administration of 0.45g/L (100mg/Kg day) and also by intraperitoneal injections of 50g/L (200mg/Kg/day) (Sun *et al*, 2010). DCA or PBS solutions were administered every day after baseline measurements. All mice were scanned at day 0 (untreated n=10 mice, treated n=8 mice), 3 days (untreated n=10 mice, treated n=8 mice) and 15 days (untreated n=7 mice, treated n=5 mice) post treatment. At each time point post treatment, three mice per group were sacrificed and tumour tissues were excised for lactate level quantification.

For MRI acquisition mice were anesthetized by injecting a mixture of tiletamine/zolazepam (Zoletil 100; Virbac, Milan, Italy) 20 mg/kg and xylazine (Rompun; Bayer, Milan, Italy) 5 mg/kg. Breath rate was monitored by an air pillow placed below the animal (SA Instruments, Stony Brook, NY; USA). MRI-CEST

pH mapping was performed upon i.v. injection of iopamidol (Bracco Imaging SpA, Colleretto Giacosa, Italy) into the tail vein at a dose of 4g I/kg b.w. through a 27-gauge needle.

MRI CEST pH-mapping acquisition and analysis

MR images were acquired with a Bruker 7T Avance 300 MRI scanner (BrukerBiospin, Ettlingen, Germany) equipped with a 30mm 1H birdcage coil before starting the treatment, after 3 and 15 days of treatment.

After the scout image acquisition, T_{2w} anatomical images were acquired with a Fast Spin Echo sequence and the same geometry was used for the following CEST experiments. CEST images were acquired with a single shot FSE sequence with centric encoding preceded by a CW-RF saturation pulse (3μT x 5s) with high in-plane resolution of 234 μm (FOV 3 cm, MTX 128, slice thickness 1.5mm). Z-spectra were acquired before and after iopamidol i.v.injection.

CEST images were analysed using homemade scripts implemented in MATLAB (The Mathworks, Inc, Natick, MA) as previously described (Terreno *et al*, 2009). Briefly, Saturation Transfer effects were calculated upon irradiating at 4.2 and at 5.5 ppm, respectively, and post-contrast ST maps were subtracted to pre-contrast ST ones, to obtain the corresponding ST contrast difference (ΔST) maps. The pixel-by-pixel extracellular pH maps were calculated using the ratio between the two contrast difference maps at 4.2 and 5.5 ppm according to the previously described method (Longo *et al*, 2011).The extracellular pH maps were superimposed to the anatomical reference image.

The heterogeneity of pHe distribution values within the tumour tissue was assessed by calculating the acidity score. The pHe values were clustered into three groups: group I consist of pixels showing pHe values > 7.0, group II of pixels showing pHe values > 6.7 and < 7.0, group III of pixels showing pHe values < 6.7. The percentage of pixels of each group was multiplied by a factor between 1 and 3, to obtain the acidity score, in accordance to the equation:

$$\textbf{Acidity Score} = \{[1 \times (\%\ of\ pixels with\ pHe > 7.0)] + [2 \times (\%pixels\ with\ 6.7 < pHe\ < 7.0)] + [3 \times (\%pixels\ with\ pHe < 6.7)]\}$$

The acidity score can range between 1 (less acidic) to 3 (more acidic).

Survival curves

Female BALB/c mice were inoculated with 2.5×10^5 TS/A cells into the right flank. After the tumour reached 1mm diameter, animals were randomized into two groups: untreated (n=9 mice) and DCA-treated (n=11 mice). DCA-treated group received DCA by oral administration (100 mg/Kg/day) and also by intraperitoneal injection (200 mg/Kg/day) every day. Untreated group received equal volumes of PBS. Mice were monitored every other day and volumes were measured using a calibre and calculated from orthogonal measurements of external dimensions as $[(width - 0.7)2 \times (length - 0.7)2]/2$. Mice were euthanized when tumour volume reached values around $600mm^3$.

Ex Vivo experiments

Lactate Assay

After MRI acquisition, three mice per each time point and group were sacrificed and tumour tissues were excised and frozen in liquid nitrogen. Tumours were assayed for lactate levels using a Lactate Assay Kit (MAK064 Sigma Aldrich, MO, USA) that determined the lactate concentration by an enzymatic reaction. Lactate concentration inside the homogenised tumour was determined measuring the absorbance at 570nm according to the manufacturer's instructions.

Statistical analysis

Calculations were performed using GraphPad Prism (GraphPad Software, La Jolla, CA, USA) software package; one-way analysis of variance was used to determine significance among groups, after which post-hoc tests with the Dunnett's Multiple Comparison Test were used for comparisons between DCA-treated and control groups. Correlation analysis were performed using Pearson's r correlation coefficient. Data are presented as mean ± SD unless otherwise stated. Statistical significance was established at $P < 0.05$.

Results

***In Vitro* experiments**

Cell viability test

In order to investigate the metabolic inhibition efficiency of DCA, a panel of breast cancer cell lines were treated with 1, 5 and 10mM of DCA (Figure1 and Supplementary 1). After 24 hours of treatment under normoxia incubation condition, all the cancer cell lines showed a reduction in their metabolic capacity. At 1mM of DCA, TS/A, TUBO and 4T1 showed a 80%-99% of vitality compared to the untreated cells; at 5mM of DCA, TUBO and 4T1 showed a 70-90 % of vitality, while TS/A showed a 63% of vitality compared to untreated cells. At 10mM of DCA, TUBO and 4T1 showed a 75% of vitality, whereas TS/A cells yielded a 58% of vitality compared to untreated cells. The response of TS/A breast cancer after 24 hour of DCA treatment was dose-dependent (Figure 1A) and significant reduction of cell vitality was already observed at the DCA concentration of 5mM. In contrast, DCA had no effect on the growth of a non-tumour control cell line, J774 (Figure 1B). On the basis of these observations, TS/A cell line was selected for subsequent studies for its higher response to the DCA treatment.

FACS analysis

In order to get more insight into how DCA affects cancer cell cycle, TS/A cells were incubated with DCA for 24 hours, then stained with PI and analysed by flow cytometry. DCA did not show to affect the cell cycle of TS/A cells into a statistically relevant extent, as the amount of cells in the G1/G0 phase decreased from 51.6% (untreated cells) to 45.9% in the presence of 10mM DCA (Supplementary Figure 2A, B). The amount of TS/A cells in the S phase did not change between untreated and treated with 10mM of DCA (Supplementary Figure 2A, C), while cells in phase G2/M increased from 18.8% (untreated cells) to 23.1% (Supplementary Figure 2A, D).

pH measurements in normoxia and hypoxia conditions

The TS/A cells were incubated in the presence of 1, 5 and 10mM of DCA for 24 hours, in both normoxic and hypoxic conditions (Figure 1C and 1D). In normoxic condition a moderate but significant and constant increase of pHe (from 7.05 to 7.24) was observed upon increasing DCA concentrations. The increase of tumour pHe was significantly more pronounced in the hypoxic condition than in the normoxic condition. Hypoxic condition resulted in lower pH of the culture medium for TS/A untreated cells in comparison to

normoxic conditions (pHe=6.75 ± 0,02 and pHe=7.05 ± 0,015 for untreated and treated cells, respectively). DCA treatment resulted in a marked increase of pHe from 6.96 to 7.53 (P<0,0001).

In Vivo experiments

Tumour growth assessment

The *in vivo* antitumour activity of DCA was evaluated by measuring the tumour volume in a group of TS/A tumour bearing BALB/c mice that received drinking water and PBS intraperitoneal injection (untreated) or that were treated with DCA by oral administration and intraperitoneal injection every day for 3 or 15 consecutive days (Figure 2A). The tumour volume was normalised by dividing the tumour volume post-treatment to the tumour volume pre-treatment. DCA treatment slightly reduced the growth of TS/A breast tumours after three days of treatment (ΔVolume% = 70.7 ± 38.6 and 83.1 ± 15.7, for treated and untreated mice, respectively; P > 0.05). This limited growth reduction is maintained up to 15 days of DCA treatment (ΔVolume% = 571.9 ± 180.7 and 646.7 ± 184.0, for untreated and treated mice, respectively; P > 0.05) (Figure 2B).

Survival curves

Intraperitoneal and oral treatments with DCA started when tumour mean volumes where ca. 60 mm^3 and terminated when tumours reached 600 mm^3 in size. DCA-treated mice survived slightly longer then the untreated mice (Figure 2C), despite not statistically significant.

MRI CEST pH-mapping

The pH-responsive contrast agent, upon extravasation inside the tumour region, allowed investigating the tumour pHe. A significant pHe increase was observed for treated mice in comparison to untreated ones after three days of DCA treatment (ΔpHe= +0.10 and -0.12 for treated and untreated, respectively, P < 0.05). The opposite pHe variations were maintained also after 15 days of treatment, despite less marked (ΔpHe= +0.003 and -0.09 for treated and untreated, respectively, Figure 3A). Representative MRI-CEST pHe images overimposed to anatomical images are shown in Figure 4 for treated and untreated mice. Following DCA-

treatment, an increase of the number of pixels with pHe values close to 7-7.4 pH unit is visible, in contrast to untreated mice at both the investigated time points (i.e. after 3 and 15 days of DCA treatment).

To assess more precisely the heterogeneity of the extracellular pH distribution inside the tumour region, it was deemed of interest to calculate an index of acidosis (the acidity score). A marked and statistically significant difference was observed in the difference of the acidity scores between untreated and treated mice after 3 days of treatment (Δacidity score = -0.14 ± 0.23 and +0.15 ± 0.34, $P < 0.005$, Figure 3B). After 15 days a marked difference in pHe distribution still remains between treated and untreated mice (Δacidity score = 0.003 ± 0.24 and 0.18 ± 0.35 for treated and untreated mice, respectively; $P > 0.05$). Representative acidity score maps are shown in Figure 5 for treated and untreated mice. Upon DCA-treatment, an increase in the number of pixels clustered around neutral pH values (colour coded in blue) is well detected after three days of treatment. Conversely, untreated mice show an increase of pixels clustered at more acidic values (colour coded in red).

Ex Vivo experiments

Lactate Assay

The tumour lactate concentration was assessed in TS/A tumour extracts. When TS/A tumour bearing mice were treated with oral and intraperitoneal DCA administration for 3 consecutive days, the lactate concentration in treated mice was significantly decreased compared with untreated ones (lactate level in treated mice is ca. 3 time lower than in untreated mice, $P = 0.0077$). No significant variation in tumour lactate levels was observed comparing treated to untreated mice after 15 days (Figure 3C). A strong and significant inverse correlation was found between lactate levels and changes in tumour pHe (Pearson's $r=-0.97$, $P < 0.05$, Figure 3D);

Discussion

High rate of glucose uptake and of lactate production are two distinctive features of metabolically altered tumour cells. DCA is able to revert the glycolytic phenotype through metabolic inhibition of PDK that allows pyruvate to enter into the tricarboxylic acid cycle thus limiting lactate production and in turn, a decrease of

H^+ ions pumped out in the extracellular space. Herein, we investigated the effect of DCA on the tumour pHe using the MRI-CEST pH imaging approach.

First of all, the *in vitro* sensitivity of different breast cancer cell lines to DCA was assessed. All cancer cell lines showed a reduction in their metabolic capacity. The TS/A cell line, that showed a dose-dependent response, was selected for further *in vivo* studies. Interestingly J774, a non-cancerous cell line, was not affected by the presence of DCA in the incubation medium, showing that DCA selectively targets cancer cells. In previous studies other breast cancer cell lines were treated with DCA (Duan *et al*, 2013; Sun *et al*, 2010). Evidences confirmed that the DCA effect on cell cycle is cellular-dependent (Wong *et al*, 2008) and studies conducted on colon rectal cancer cells revealed that DCA treatment at 20mM concentration caused apoptosis and G2 phase cell-cycle arrest (Madhok *et al*, 2010). We observed a similar behaviour in TS/A cells, although the slight decrease in G2/M phase induced by DCA in our model did not appear statistically significant.

Assessment of the glycolytic inhibitory effect of DCA on tumour cells has been usually carried out *in vitro* studies by measuring pHe changes. Our *in vivo* MRI-based observations correlate well with the *in vitro* studies as they show a significant increase in the pHe following the DCA treatment. The alkalinisation of the pHe was even more pronounced when TS/A cells were cultured in hypoxic conditions (1% O_2), simulating a poorly-perfused tumour microenvironment. We observed a similar shift of the deregulated metabolism in treated mice as earlier as three days after the application of the DCA-treatment.

Decreased oxygen availability (hypoxia) stimulates cells to consume glucose and produce lactate. Lactate is taken up by surrounding tumour cells with reciprocal recycling to support the growth of the tumour and resistance to apoptotic cell death mechanisms (DeBerardinis *et al*, 2008). Other studies in breast, prostate, colorectal cancer cell lines showed that lactate production is reduced upon DCA treatment (Kailavasan *et al*, 2014; Lefort *et al*, 2014; Lin *et al*, 2014; Robey & Martin, 2011; Xintaropoulou *et al*, 2015). We observed a similar decrease in lactate levels after three days of treatment. Notably, these changes in lactate levels were correlated with changes in tumour pHe. Treated mice showed lower lactate levels and lower acidification after 3 days of treatment as compared to untreated mice.

Interestingly, despite DCA treated mice showed a limited tumour growth following 15 days of treatment, only a slight increase of the survival time was observed as compared to untreated mice. It is known that DCA alone has a moderate efficiency as chemotherapeutic drug, as its antineoplastic pharmacological effect can be augmented when used in combination with other drugs (Haugrud *et al*, 2014; Robey & Martin, 2011; Sanchez *et al*, 2013; Stander *et al*, 2015). Our results are in agreement with these observations, as similar lactate levels were observed in untreated and treated mice after 15 days of treatment. These results parallel those obtained by measuring *in vivo* tumour pHe, which at 15 days show a reduced difference between treated and untreated mice in terms of pHe changes and of acidity scores. These findings confirm the ability of the proposed non-invasive approach to assess the onset of resistance to DCA, since tumour acidosis, despite significantly reduced after 3 days of treatment, returned to almost baseline values after 15 days. This behaviour was confirmed by similar changes in lactate levels. Moreover, the inefficacy of DCA to halt tumour glycolysis after 15 days, as measured by the proposed approach, anticipated the lack of difference in terms of survival times between treated and untreated groups.

In this study, *in vivo* pH changes were assessed by MRI-CEST imaging using iopamidol, a MRI-CEST pH-responsive agents able to map pHe and tumour perfusion in the microenvironment in which it distributes (Anemone *et al*, 2016; Longo *et al*, 2016b; Longo *et al*, 2014). Although iopamidol showed a heterogeneous distribution in the tumour region, the application of the ratiometric pH method allowed obtaining representative pH maps for the region of interest. To get more insight into the tumour pHe heterogeneity we calculated the acidity score that reports on the distribution of pixels aggregated on the basis of their relative acidity inside the tumour region. Representative treated mice acidity score maps showed an increase in blue pixel during DCA treatment, reflecting the DCA-induced glycolysis inhibition, hence alkalinisation of tumour pHe. A similar decrease of tumour acidosis was observed in a xenograft model of B-cell lymphoma upon treatment with metaiodobenzylguanidine by using an analogous pH-responsive CEST agent (Chen *et al*, 2015). Interestingly, also endogenous CEST pH mapping allows to monitor intracellular acidification following Lonidamine or Topiramate treatment in orthotopic glyoblastoma tumors (Marathe *et al*, 2016; McVicar *et al*, 2015). All these results confirm the feasibility of MRI-CEST pH mapping to monitor the response to drugs targeting tumour metabolism.

In conclusion, this study demonstrated that MRI-CEST pH imaging is able to detect the early therapeutic response to DCA by measuring changes in tumour pHe that correlate well with the observed reduced lactate levels as a consequence of the reversed glycolytic phenotype. These results suggest that MRI-CEST pH imaging may serve as a useful imaging biomarker for monitoring treatment response to drugs targeting tumour deregulated glycolysis.

Acknowledgments

Financial support from European Community `s Seventh Framework Programme (FP7 GLINT project 602306) is gratefully acknowledged. L. Conti was supported by a fellowship from Fondazione Umbero Veronesi.

Titles and legends to figures

Figure1. Effect of DCA on cell growth. **(A and B)** Percentage of vitality of TS/A (A) and J774 (B) cells after 24 hours of DCA treatment. **(C and D)** extracellular pH measurement after 24 hours of DCA treatment for TS/A cells grown in normoxic (C) or in hypoxic (D; 1% O_2) conditions. *P < 0.05; ***P < 0.0001, Dunnett's Multiple Comparison Test.

Figure2. Effect of DCA on tumour growth in vivo. **(A**) Normalised and (B) delta volume % of TS/A tumour bearing mice before and after 3 or 15 days of DCA treatment. (**C**) Mice survival curve after DCA treatment.

Figure3. Tumour pHe (**A**) and acidity score (**B**) changes calculated from TS/A tumour bearing mice upon DCA treatment after 3 and 15 days, in comparison to before treatment tumour pHe values for untreated and treated mice. (**C**) Lactate quantification from excised TS/A tumour tissues for untreated and treated mice after3 days and 15 days of DCA treatment. (**D**) Correlation between changes in tumour pHe and normalised lactate concentration (Pearson r = -0,97).

Figure 4. Representative tumour pHe maps superimposed on anatomical images at baseline (top right), 3 days (bottom left) and 15 days (bottom right) post DCA treatment for untreated (**A**) and treated mouse (**B**).

Figure 5. Representative tumour extracellular acidty maps at baseline (top right), 3 days (bottom left) and 15 days (bottom right) post DCA treatment superimposed on anatomical images for untreated (**A**) and treated mouse (**B**).

References

Anemone A, Consolino L, Longo DL (2016) MRI-CEST assessment of tumour perfusion using X-ray iodinated agents: comparison with a conventional Gd-based agent. *European radiology* DOI: 10.1007/s00330-016-4552-7

Bonnet S, Archer SL, Allalunis-Turner J, Haromy A, Beaulieu C, Thompson R, Lee CT, Lopaschuk GD, Puttagunta L, Bonnet S, Harry G, Hashimoto K, Porter CJ, Andrade MA, Thebaud B, Michelakis ED (2007) A mitochondria-K+ channel axis is suppressed in cancer and its normalization promotes apoptosis and inhibits cancer growth. *Cancer cell* **11**(1)**:** 37-51

Chen LQ, Howison CM, Jeffery JJ, Robey IF, Kuo PH, Pagel MD (2014) Evaluations of extracellular pH within in vivo tumors using acidoCEST MRI. *Magn Reson Med* **72**(5)**:** 1408-17

Chen LQ, Howison CM, Spier C, Stopeck AT, Malm SW, Pagel MD, Baker AF (2015) Assessment of carbonic anhydrase IX expression and extracellular pH in B-cell lymphoma cell line models. *Leukemia & lymphoma* **56**(5)**:** 1432-9

Chu QS, Sangha R, Spratlin J, Vos LJ, Mackey JR, McEwan AJ, Venner P, Michelakis ED (2015) A phase I open-labeled, single-arm, dose-escalation, study of dichloroacetate (DCA) in patients with advanced solid tumors. *Investigational new drugs* **33**(3)**:** 603-10

DeBerardinis RJ, Lum JJ, Hatzivassiliou G, Thompson CB (2008) The biology of cancer: metabolic reprogramming fuels cell growth and proliferation. *Cell metabolism* **7**(1)**:** 11-20

Duan Y, Zhao X, Ren W, Wang X, Yu KF, Li D, Zhang X, Zhang Q (2013) Antitumor activity of dichloroacetate on C6 glioma cell: in vitro and in vivo evaluation. *OncoTargets and therapy* **6:** 189-98

Dunbar EM, Coats BS, Shroads AL, Langaee T, Lew A, Forder JR, Shuster JJ, Wagner DA, Stacpoole PW (2014) Phase 1 trial of dichloroacetate (DCA) in adults with recurrent malignant brain tumors. *Investigational new drugs* **32**(3)**:** 452-64

Gallagher FA, Kettunen MI, Day SE, Hu DE, Ardenkjaer-Larsen JH, Zandt R, Jensen PR, Karlsson M, Golman K, Lerche MH, Brindle KM (2008) Magnetic resonance imaging of pH in vivo using hyperpolarized 13C-labelled bicarbonate. *Nature* **453**(7197)**:** 940-3

Garcia-Martin ML, Martinez GV, Raghunand N, Sherry AD, Zhang S, Gillies RJ (2006) High resolution pH(e) imaging of rat glioma using pH-dependent relaxivity. *Magn Reson Med* **55**(2)**:** 309-15

Garon EB, Christofk HR, Hosmer W, Britten CD, Bahng A, Crabtree MJ, Hong CS, Kamranpour N, Pitts S, Kabbinavar F, Patel C, von Euw E, Black A, Michelakis ED, Dubinett SM, Slamon DJ (2014) Dichloroacetate should be considered with platinum-based chemotherapy in hypoxic tumors rather than as a single agent in advanced non-small cell lung cancer. *Journal of cancer research and clinical oncology* **140**(3)**:** 443-52

Gerweck LE, Seetharaman K (1996) Cellular pH gradient in tumor versus normal tissue: potential exploitation for the treatment of cancer. *Cancer research* **56**(6)**:** 1194-8

Gillies RJ, Liu Z, Bhujwalla Z (1994) 31P-MRS measurements of extracellular pH of tumors using 3-aminopropylphosphonate. *The American journal of physiology* **267**(1 Pt 1)**:** C195-203

Hashim AI, Zhang X, Wojtkowiak JW, Martinez GV, Gillies RJ (2011) Imaging pH and metastasis. *NMR in biomedicine* **24**(6)**:** 582-91

Haugrud AB, Zhuang Y, Coppock JD, Miskimins WK (2014) Dichloroacetate enhances apoptotic cell death via oxidative damage and attenuates lactate production in metformin-treated breast cancer cells. *Breast cancer research and treatment* **147**(3)**:** 539-50

Hingorani DV, Bernstein AS, Pagel MD (2015) A review of responsive MRI contrast agents: 2005-2014. *Contrast media & molecular imaging* **10**(4)**:** 245-65

Jones KM, Randtke EA, Howison CM, Cardenas-Rodriguez J, Sime PJ, Kottmann MR, Pagel MD (2015) Measuring extracellular pH in a lung fibrosis model with acidoCEST MRI. *Molecular imaging and biology : MIB : the official publication of the Academy of Molecular Imaging* **17**(2)**:** 177-84

Kailavasan M, Rehman I, Reynolds S, Bucur A, Tozer G, Paley M (2014) NMR-based evaluation of the metabolic profile and response to dichloroacetate of human prostate cancer cells. *NMR in biomedicine* **27**(5)**:** 610-6

Kinnaird A, Michelakis ED (2015) Metabolic modulation of cancer: a new frontier with great translational potential. *Journal of molecular medicine* **93**(2)**:** 127-42

Lanzardo S, Conti L, Rooke R, Ruiu R, Accart N, Bolli E, Arigoni M, Macagno M, Barrera G, Pizzimenti S, Aurisicchio L, Calogero RA, Cavallo F (2016) Immunotargeting of Antigen xCT Attenuates Stem-like Cell Behavior and Metastatic Progression in Breast Cancer. *Cancer research* **76**(1)**:** 62-72

Lefort N, Brown A, Lloyd V, Ouellette R, Touaibia M, Culf AS, Cuperlovic-Culf M (2014) (1)H NMR metabolomics analysis of the effect of dichloroacetate and allopurinol on breast cancers. *Journal of pharmaceutical and biomedical analysis* **93:** 77-85

Lin G, Hill DK, Andrejeva G, Boult JK, Troy H, Fong AC, Orton MR, Panek R, Parkes HG, Jafar M, Koh DM, Robinson SP, Judson IR, Griffiths JR, Leach MO, Eykyn TR, Chung YL (2014) Dichloroacetate induces autophagy in colorectal cancer cells and tumours. *British journal of cancer* **111**(2)**:** 375-85

Longo DL, Bartoli A, Consolino L, Bardini P, Arena F, Schwaiger M, Aime S (2016a) In vivo imaging of tumour metabolism and acidosis by combining PET and MRI-CEST pH imaging. *Cancer research DOI: 10.1158/0008-5472.CAN-16-0825*

Longo DL, Busato A, Lanzardo S, Antico F, Aime S (2013) Imaging the pH evolution of an acute kidney injury model by means of iopamidol, a MRI-CEST pH-responsive contrast agent. *Magn Reson Med* **70**(3)**:** 859-64

Longo DL, Dastru W, Digilio G, Keupp J, Langereis S, Lanzardo S, Prestigio S, Steinbach O, Terreno E, Uggeri F, Aime S (2011) Iopamidol as a responsive MRI-chemical exchange saturation transfer contrast agent for pH mapping of kidneys: In vivo studies in mice at 7 T. *Magn Reson Med* **65**(1)**:** 202-11

Longo DL, Michelotti F, Consolino L, Bardini P, Digilio G, Xiao G, Sun PZ, Aime S (2016b) In Vitro and In Vivo Assessment of Nonionic Iodinated Radiographic Molecules as Chemical Exchange Saturation Transfer Magnetic Resonance Imaging Tumor Perfusion Agents. *Investigative radiology* **51**(3)**:** 155-62

Longo DL, Sun PZ, Consolino L, Michelotti FC, Uggeri F, Aime S (2014) A general MRI-CEST ratiometric approach for pH imaging: demonstration of in vivo pH mapping with iobitridol. *Journal of the American Chemical Society* **136**(41)**:** 14333-6

Madhok BM, Yeluri S, Perry SL, Hughes TA, Jayne DG (2010) Dichloroacetate induces apoptosis and cell-cycle arrest in colorectal cancer cells. *British journal of cancer* **102**(12)**:** 1746-52

Marathe K, McVicar N, Li A, Bellyou M, Meakin S, Bartha R (2016) Topiramate induces acute intracellular acidification in glioblastoma. *Journal of neuro-oncology* DOI: 10.1007/s11060-016-2258-y

McFate T, Mohyeldin A, Lu H, Thakar J, Henriques J, Halim ND, Wu H, Schell MJ, Tsang TM, Teahan O, Zhou S, Califano JA, Jeoung NH, Harris RA, Verma A (2008) Pyruvate dehydrogenase complex activity controls metabolic and malignant phenotype in cancer cells. *The Journal of biological chemistry* **283**(33)**:** 22700-8

McVicar N, Li AX, Meakin SO, Bartha R (2015) Imaging chemical exchange saturation transfer (CEST) effects following tumor-selective acidification using lonidamine. *NMR in biomedicine* **28**(5)**:** 566-75

Michelakis ED, Webster L, Mackey JR (2008) Dichloroacetate (DCA) as a potential metabolic-targeting therapy for cancer. *British journal of cancer* **99**(7)**:** 989-94

Moon BF, Jones KM, Chen LQ, Liu P, Randtke EA, Howison CM, Pagel MD (2015) A comparison of iopromide and iopamidol, two acidoCEST MRI contrast media that measure tumor extracellular pH. *Contrast media & molecular imaging* **10**(6)**:** 446-55

Nanni P, de Giovanni C, Lollini PL, Nicoletti G, Prodi G (1983) TS/A: a new metastasizing cell line from a BALB/c spontaneous mammary adenocarcinoma. *Clinical & experimental metastasis* **1**(4)**:** 373-80

Reineri F, Boi T, Aime S (2015) ParaHydrogen Induced Polarization of 13C carboxylate resonance in acetate and pyruvate. *Nat Commun* **6:** 5858

Reineri F, Daniele V, Cavallari E, Aime S (2016) Assessing the transport rate of hyperpolarized pyruvate and lactate from the intra- to the extracellular space. *NMR Biomed* **29**(8)**:** 1022-7

Robey IF, Martin NK (2011) Bicarbonate and dichloroacetate: evaluating pH altering therapies in a mouse model for metastatic breast cancer. *BMC cancer* **11:** 235

Sanchez WY, McGee SL, Connor T, Mottram B, Wilkinson A, Whitehead JP, Vuckovic S, Catley L (2013) Dichloroacetate inhibits aerobic glycolysis in multiple myeloma cells and increases sensitivity to bortezomib. *British journal of cancer* **108**(8)**:** 1624-33

Serrao EM, Brindle KM (2016) Potential Clinical Roles for Metabolic Imaging with Hyperpolarized [1-(13)C]Pyruvate. *Front Oncol* **6:** 59

Stander XX, Stander BA, Joubert AM (2015) Synergistic anticancer potential of dichloroacetate and estradiol analogue exerting their effect via ROS-JNK-Bcl-2-mediated signalling pathways. *Cellular physiology and biochemistry : international journal of experimental cellular physiology, biochemistry, and pharmacology* **35**(4)**:** 1499-526

Sun RC, Fadia M, Dahlstrom JE, Parish CR, Board PG, Blackburn AC (2010) Reversal of the glycolytic phenotype by dichloroacetate inhibits metastatic breast cancer cell growth in vitro and in vivo. *Breast cancer research and treatment* **120**(1)**:** 253-60

Terreno E, Stancanello J, Longo D, Castelli DD, Milone L, Sanders HM, Kok MB, Uggeri F, Aime S (2009) Methods for an improved detection of the MRI-CEST effect. *Contrast media & molecular imaging* **4**(5)**:** 237-47

Viale A, Reineri F, Dastru W, Aime S (2012) Hyperpolarized (13)C-pyruvate magnetic resonance imaging in cancer diagnostics. *Expert Opin Med Diagn* **6**(4)**:** 335-45

Warburg O, Wind F, Negelein E (1927) The Metabolism of Tumors in the Body. *The Journal of general physiology* **8**(6)**:** 519-30

Webb BA, Chimenti M, Jacobson MP, Barber DL (2011) Dysregulated pH: a perfect storm for cancer progression. *Nature reviews Cancer* **11**(9)**:** 671-7

Wong JY, Huggins GS, Debidda M, Munshi NC, De Vivo I (2008) Dichloroacetate induces apoptosis in endometrial cancer cells. *Gynecologic oncology* **109**(3)**:** 394-402

Xintaropoulou C, Ward C, Wise A, Marston H, Turnbull A, Langdon SP (2015) A comparative analysis of inhibitors of the glycolysis pathway in breast and ovarian cancer cell line models. *Oncotarget* **6**(28)**:** 25677-95

Zhang X, Lin Y, Gillies RJ (2010) Tumor pH and its measurement. *Journal of nuclear medicine : official publication, Society of Nuclear Medicine* **51**(8)**:** 1167-70

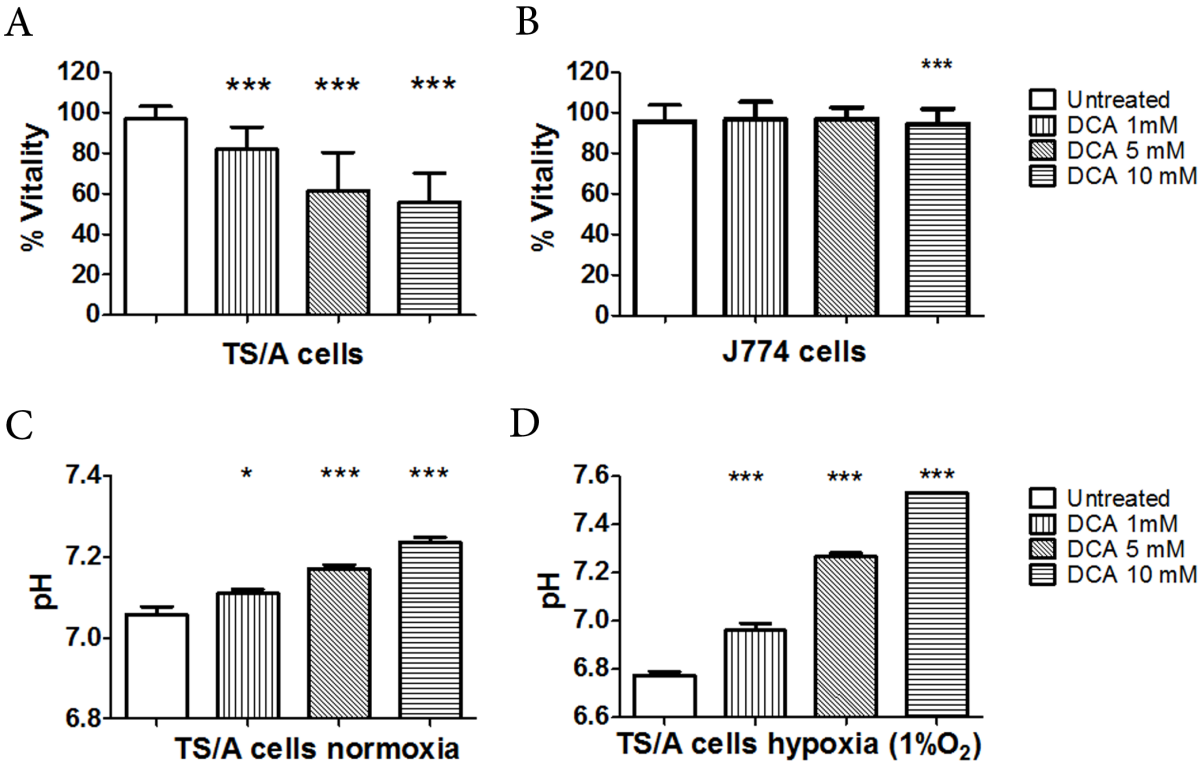
A
B
C
D
% Vitality
TS/A cells
J774 cells
pH
TS/A cells normoxia
TS/A cells hypoxia (1%O2)
Untreated
DCA 1mM
DCA 5 mM
DCA 10 mM
***
*

A

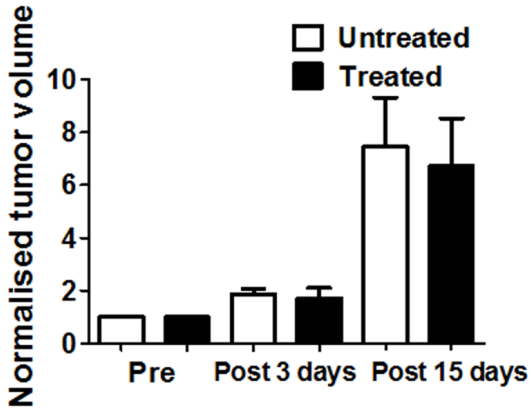
Untreated
Treated
Normalised tumor volume
0
2
4
6
8
10
Pre
Post 3 days
Post 15 days

B

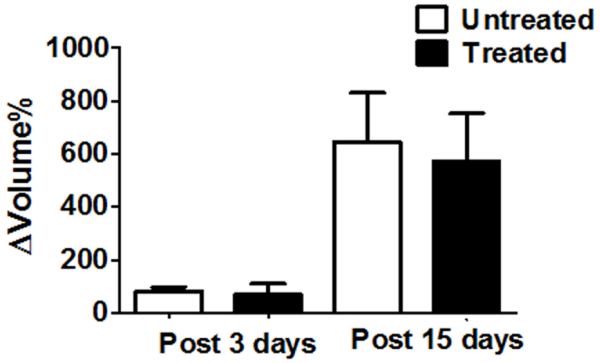
Untreated
Treated
ΔVolume%
0
200
400
600
800
1000
Post 3 days
Post 15 days

C

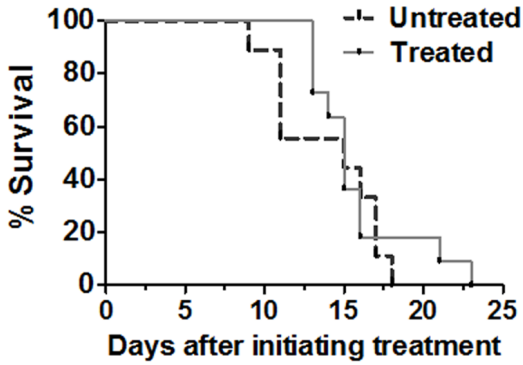
Untreated
Treated
% Survival
0
20
40
60
80
100
0
5
10
15
20
25
Days after initiating treatment

A

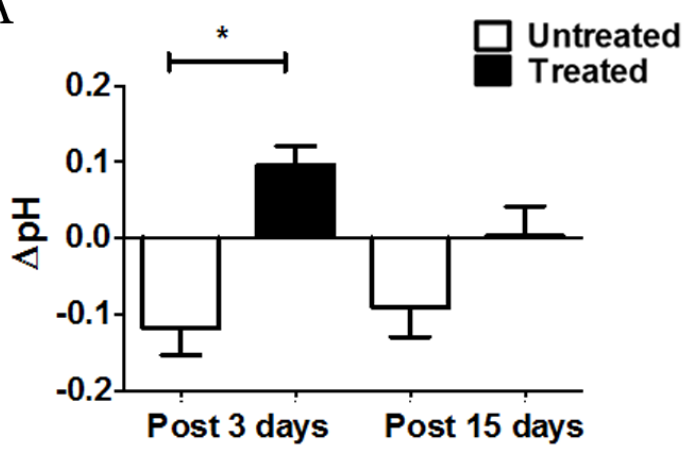
*
Untreated
Treated
0.2
0.1
0.0
-0.1
-0.2
ΔpH
Post 3 days
Post 15 days

B

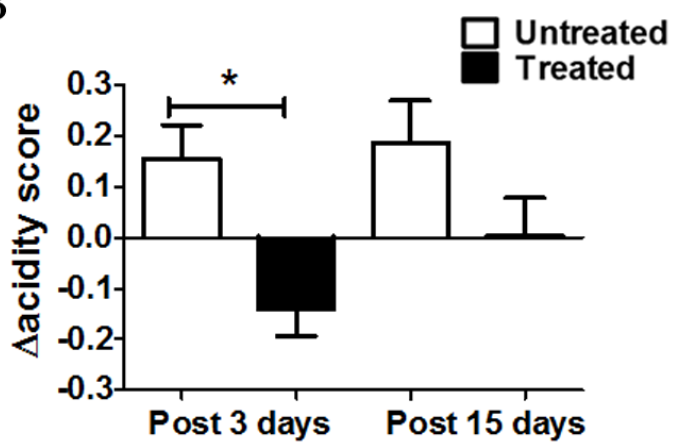
*
Untreated
Treated
0.3
0.2
0.1
0.0
-0.1
-0.2
-0.3
Δacidity score
Post 3 days
Post 15 days

C

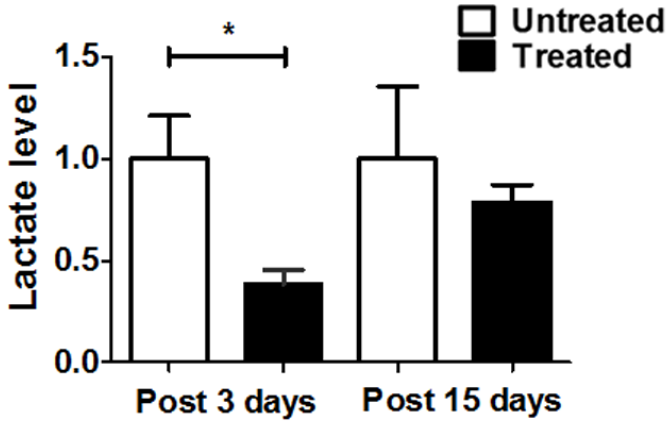
*
Untreated
Treated
1.5
1.0
0.5
0.0
Lactate level
Post 3 days
Post 15 days

D

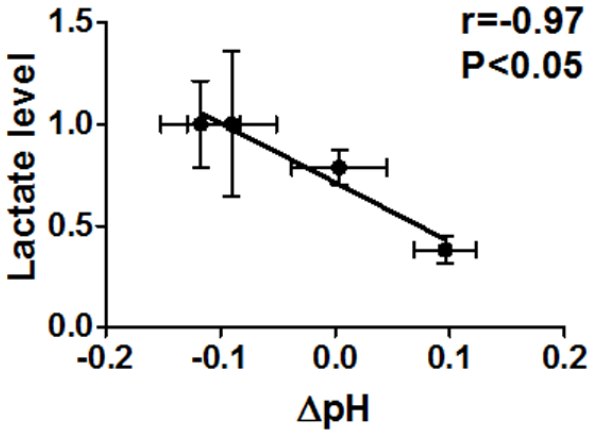
r=-0.97
P<0.05
1.5
1.0
0.5
0.0
Lactate level
-0.2
-0.1
0.0
0.1
0.2
ΔpH

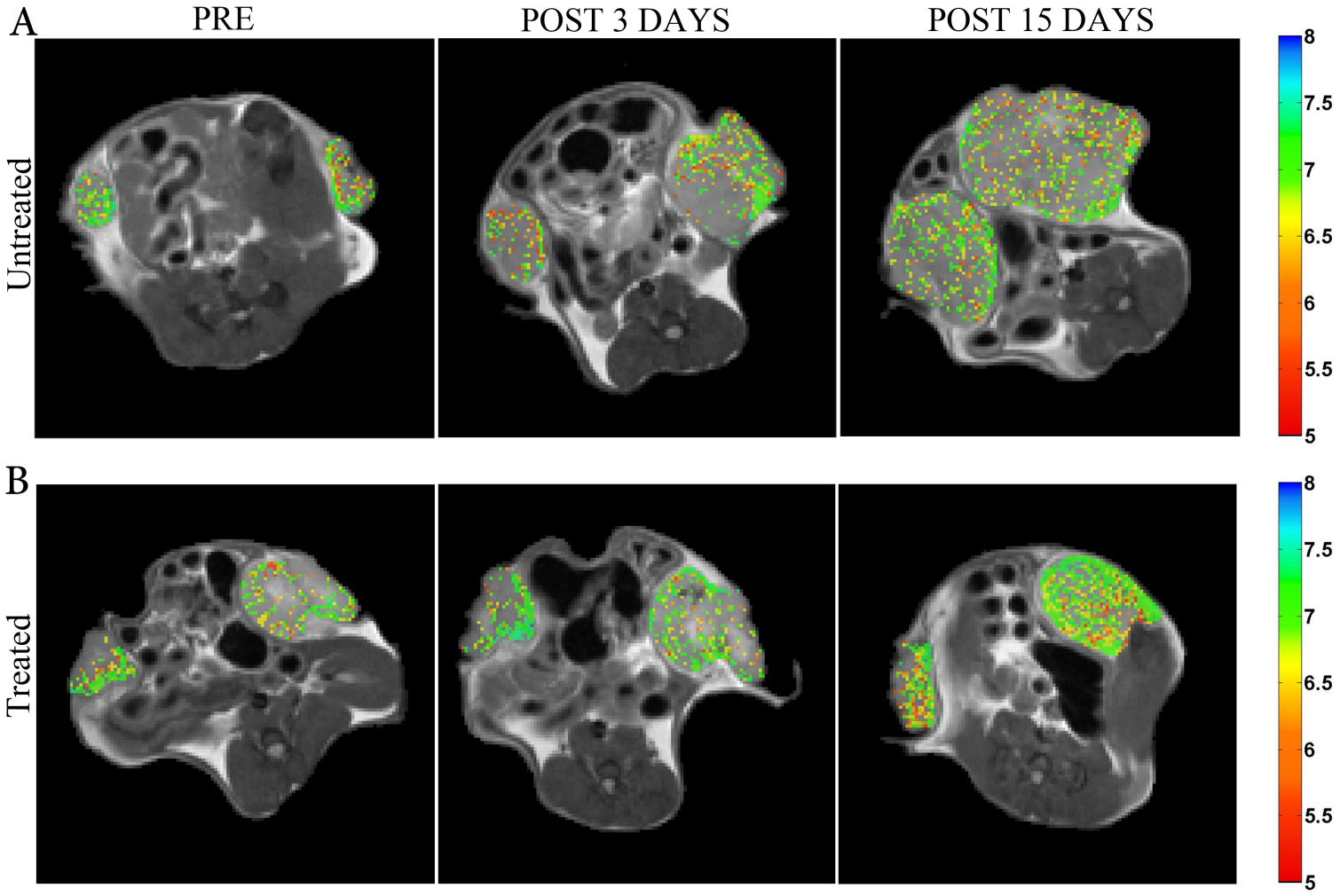
A
PRE
POST 3 DAYS
POST 15 DAYS
Untreated
B
Treated
8
7.5
7
6.5
6
5.5
5

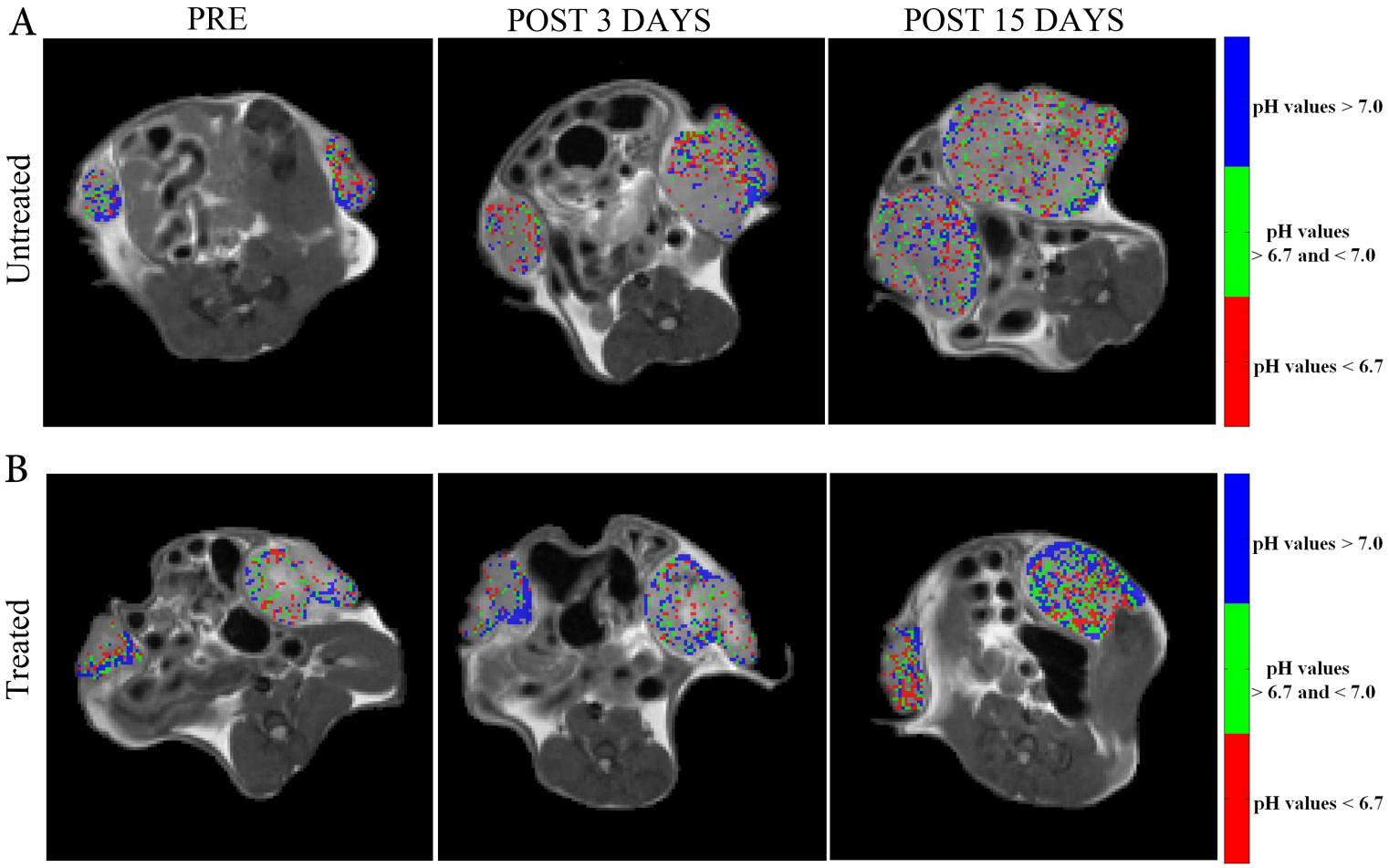
A
PRE
POST 3 DAYS
POST 15 DAYS
Untreated
pH values > 7.0
pH values > 6.7 and < 7.0
pH values < 6.7
B
Treated
pH values > 7.0
pH values > 6.7 and < 7.0
pH values < 6.7